https://doi.org/10.5194/essd-2026-427
Preprint. Discussion started: 23 June 2026

Open Access Earth System Science Data Discussions

Experimental dataset on estuarine hydrodynamics and morphodynamics for various planforms, perturbations and timescales

Eise W. Nota[1], Yinghua Li[1], Lotta Beyaard[1], Meryem Upson[1,2], Menno L.C. Wagenaar[1], Zahra Nassralla[1], Silke J. Baltussen[1], Esmee van Amelsfort[1], Lieke M. Gubbels[1], David Leahy[1], Janneke J. Muller[1], Brechtje A. van Amstel[1], Josefien J.A. Donders[1], Jan-Eike Rossius[1,3], Marcel C.G. van Maarseveen[4], Henk Markies[4], Arjan M. van Eijk[4], Bas D.B van Dam[4], Madlene Nussbaum[1], Saeb Faraji Gargari[1], Vincent Brunst[5], Lisanne Braat[1], and Maarten G. Kleinhans[1]

[1]Department of Physical Geography, Utrecht University, Utrecht, the Netherlands
[2]Marine and Environmental Biogeosciences Research Group, Universitat Autónoma de Barcelona, Barcelona, Spain
[3]Department of Marine Sciences, University of Gothenburg, Fiskebäckskil, Sweden
[4]Earth Simulation Laboratory, Utrecht University, Utrecht, the Netherlands
[5]Faculty of Geosciences, Utrecht University, Utrecht, the Netherlands

Correspondence: Eise W. Nota (e.w.nota@uu.nl)

Abstract.

It is increasingly important to better understand the hydrodynamic and morphodynamic processes of estuaries, because climate change, sea level rise, and human activities cause perturbations and forcing that can be detrimental to coastal ecosystems and communities. It is however challenging to obtain comprehensive data of natural processes in estuaries, due to their highly dynamic nature induced by daily reversing tidal flows, and morphological change occurring over various spatial scales and timescales, ranging from tidal cycles to decades. Conducting physical scale experiments in laboratory flumes is a means to overcome these challenges, as they allow for rapid morphological development and plenty of measurement opportunities.

In this work we present a large, publicly available dataset of 19 morphological experiments of estuaries in the Metronome tidal facility (www.uu.nl/Metronome), covering almost 230,000 emulated tidal cycles ($T = 40$ s). The dataset comprises experiments with fixed perturbations in planform shape or tidal settings, temporary perturbations in initial bed morphology, and repeat experiments under the same boundary conditions. Besides, there are two complementary river experiments. The available data consists of planform masks, distributed laserscan DEMs, as well as temporally dense timelapses, orthomosaics and water depth maps computed from overhead imagery taken at fixed moments every 20 tidal cycles. Furthermore, there are occasional orthomosaics and water depth maps from 1 Hz timelapse imagery taken during several consecutive tidal cycles, and orthomosaics from 25 Hz imagery with floating plastic particles, allowing for Particle Image Velocimetry (PIV). All data has been processed through recently developed methods involving a fixed base model geometry, assuring optimal spatial and relative accuracies. The dataset allows for advancements in numerous disciplines studying estuaries, such as morphology, bar theory, chaos theory, channel network analysis, machine learning, and calibration of coastal numerical models. The dataset can be accessed through https://public.yoda.uu.nl/geo/UU01/KKEUY5.html (Nota et al., 2026a).

https://doi.org/10.5194/essd-2026-427
Preprint. Discussion started: 23 June 2026

Open Access Earth System Science Data Discussions

1 Introduction

Estuaries are the confined downstream areas of rivers ending in the sea, dominated by rapidly changing reversing tidal flows (Kennish, 2002). In combination with upstream river discharge, these tidal flows induce complex patterns of water flow, sediment transport and morphological development. These processes all occur on multiple timescales, ranging from tidal cycles (Montani et al., 1998), to seasonal cycles (Nowacki et al., 2015), to longer timescales in the order of decades (Elias et al., 2023). The hydrodynamic and morphodynamic processes of estuaries have profound effects on the numerous stakeholders that depend on them, such as protected ecosystems, coastal communities, critical infrastructure, and industries. It is therefore imperative to study estuarine hydrodynamic and morphodynamic processes on these different timescales. This is increasingly urgent considering the effects of climate change, sea level rise, and often far-reaching human activities, which can impose detrimental temporary or permanent perturbations on these highly dynamic systems (Kennish, 2002; Clark et al., 2016; Leuven et al., 2019; Cox et al., 2022; Van Maren et al., 2023). However, it remains challenging to study the processes of these landscapes on a system scale, due to the highly dynamic nature of estuaries on these various timescales, as well as the practical and financial constraints of frequently conducting field surveys (Van der Wal and Pye, 2003; Dorst et al., 2013; Elias et al., 2023; Lin et al., 2026). For example, the costs of a single bathymetry survey of the Western Scheldt estuary in the Netherlands are of the order of a million euro. Accordingly, estuarine processes and their interactions, in particular the complex relation between natural and human-induced sediment dynamics and long-term morphological developments under changing boundary conditions, are limitedly understood, which also complicates numerical modelling of these systems and validation thereof (Cea and French, 2012; Clark et al., 2016; Williams and Esteves, 2017; Baar et al., 2019).

Challenges of studying morphodynamic processes in natural systems can be addressed by conducting physical scale experiments, wherein morphological features such as bars and channels develop rapidly. Moreover, such experiments allow for frequent and complete measurements under controlled conditions, and opportunities to collect large datasets (Paola et al., 2009; Kleinhans et al., 2014; Leenman and Eaton, 2024). For estuaries specifically, physical scale experiments have a long but slim history (Reynolds, 1888; Reynolds et al., 1901), notwithstanding particular challenges for successfully conducting them.

First, it is important to consider the spatial and temporal scaling of natural systems to a laboratory scale in order to obtain meaningful experimental results (Paola et al., 2009). For physical scale experiments involving bed load sediment transport, the Shields number is often considered critical (Kleinhans, 2005; Kleinhans et al., 2014). For experimental rivers, Shields scaling allows for scaled bed load transport by increasing the slope of a laboratory facility, as compared to natural systems, causing the sediment transport capacity of water flow to increase (Kleinhans et al., 2014). However, for experimental estuaries, reversing tidal flows complicate such scaling, restricting researchers to use finer grain sizes, which lead to aggravating scale effects of scours and ripples that are not scalable (Kleinhans et al., 2017a). To counter these undesired scale effects by using coarser sand, whilst maintaining properly scaled sediment transport and morphology, our laboratory facility incorporates periodic tilting (Kleinhans et al., 2015, 2017b; Leuven et al., 2018; Braat et al., 2019), and is hence referred to as the Metronome (www.uu.nl/metronome).

https://doi.org/10.5194/essd-2026-427
Preprint. Discussion started: 23 June 2026

Open Access Earth System Science Data Discussions

Second, and often limitedly addressed, are the uncertainties of the laboratory instrumentation and their relative alignment, which can lead to significant biases and misalignment of processed data and leave in unwanted artifacts that thwart automated data analyses (Nota et al., 2026d), such as can be conducted with numerical model output. We recently developed methods for our facility that addressed these issues and allowed us to optimize and reliably quantify uncertainties of processed data (Nota et al., 2026d). These improvements in data processing allowed us to apply machine learning to quantify water depths from imagery of our experimental facility (Nota et al., 2026b).

In this work we present a dataset, now publicly available, of estuarine experiments that have been processed through our recently developed methods (Nota et al., 2026b, d), and that we conducted over the course of almost four years. These experiments consist of self-forming sandy estuaries of various planforms that are subjected to various perturbations, boundary conditions and topographic forcing conditions, and are suitable for quantitative studies over various timescales. This dataset is part of the Delta-ENIGMA research infrastructure project (https://delta-enigma.nl/work-package-labs/) that forms a framework of instruments, data, facilities and knowledge on rivers, estuaries, coasts and dunes in the Netherlands (Dutta et al., 2026), and is embedded within the European DANUBIUS-RI (Bradley et al., 2018). Within this framework, access to the Metronome facility can be requested. In this paper, we first report on the experimental facility, instrumentation and data processing methods in more detail. Then we describe the dataset and highlight research opportunities that it enables.

2 Metronome facility

The Metronome is a 20 by 3 m laboratory flume that is used for physical scale experiments of coastal and riverine systems, allowing for morphological development of landscapes through river and tidal flows (Fig. 1; Kleinhans et al., 2017b). Here we only describe the setups for experimental estuaries, which are designed to emulate morphology scales between 1:100 and 1:10,000. The initial conditions in these experiments are typically prepared by smoothening a channel in a sandy bed using a supporting cart that is movable along the x-axis of the facility (Fig. 1.a). During an experiment, water is pumped from a water storage reservoir into: (i) a closed river boundary at $x = 0$ m; and (ii) an open sea boundary at $x > 18$ m (Fig. 1.a&d). Sea level is controlled by an adjustable overflowing weir at the open end of the sea boundary, of which motion is synchronized to the tilting (detailed below).

In order to observe water depths, we add blue dye (Brilliant Blue FCF) to the water. We assure consistent dye concentrations by following a spectrophotometric protocol, involving daily dye concentration measurements, and manual recharge of dye to desired concentration when required (Nota et al., 2026b).

Experimental reversing flows that represent tidal currents are generated by periodic tilting over the short axis of the flume at $x = 10$ m, with a fixed period of $T = 40$ s. We applied two different tidal settings: (i) asymmetric tide, following a flood-dominant curve; and (ii) symmetric tide, being equally divided between ebb and flood stage. Eq. 1 provides the tilt function to describe the $z_{x,t}$ position (in m) of the flume at any second t along the x-axis.

https://doi.org/10.5194/essd-2026-427
Preprint. Discussion started: 23 June 2026

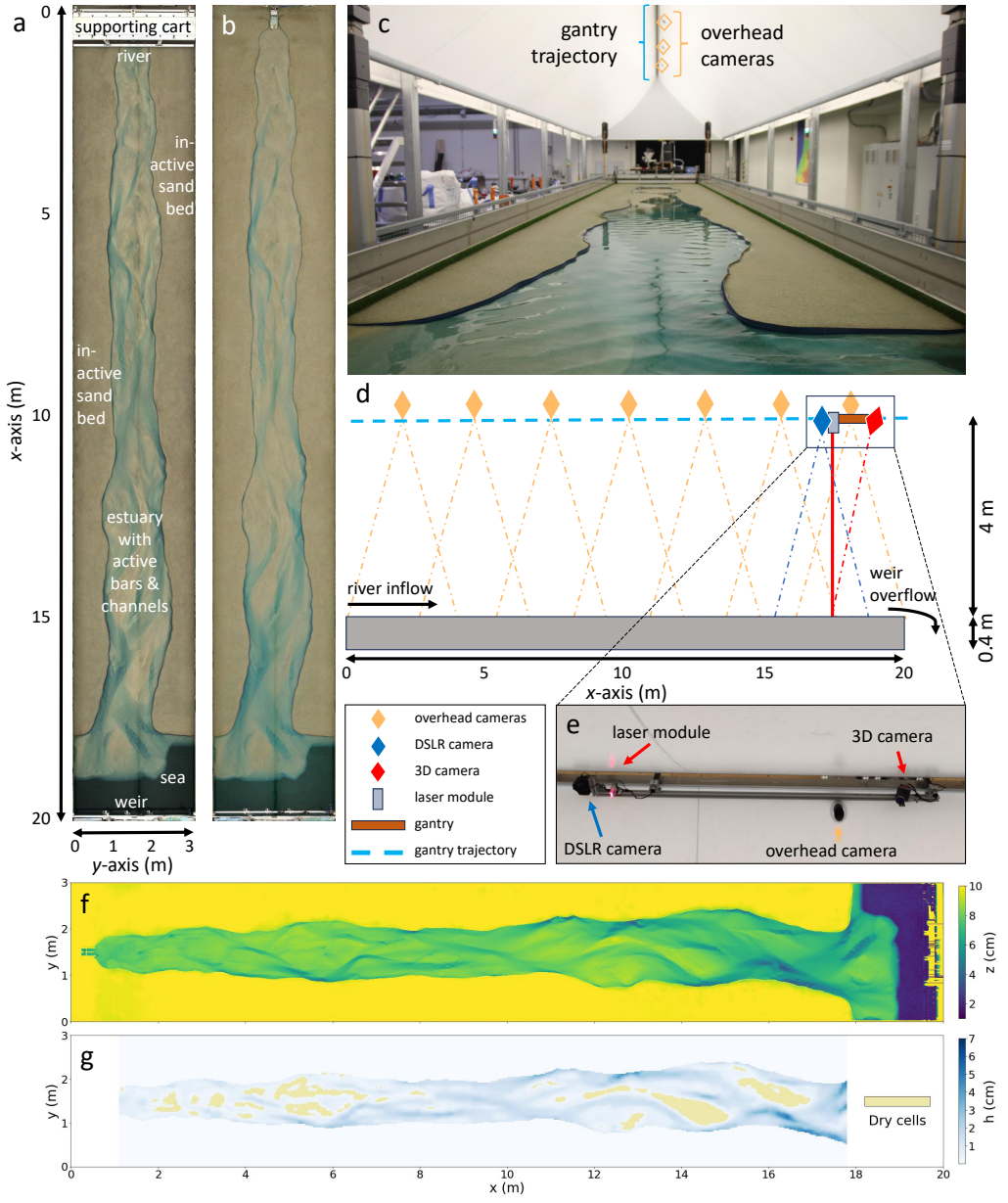

Figure 1. Overview of Metronome facility, instrumentation and processed data available in the dataset. (a) *Interval* overhead orthomosaic. (b) DSLR orthomosaic. (c) Oblique view of the facility looking from the sea in the front to the river boundary in the back. (d) Sideward sketch of the facility with relevant sensors. (e) Photograph of the gantry with sensors indicated against the tent ceiling for uniform lighting. (f) Laserscan DEM. (g) Water depth map calculated from the overhead orthomosaic at panel a at 25 mm resolution after the experimental planform mask is applied (Nota et al., 2026b).

https://doi.org/10.5194/essd-2026-427
Preprint. Discussion started: 23 June 2026

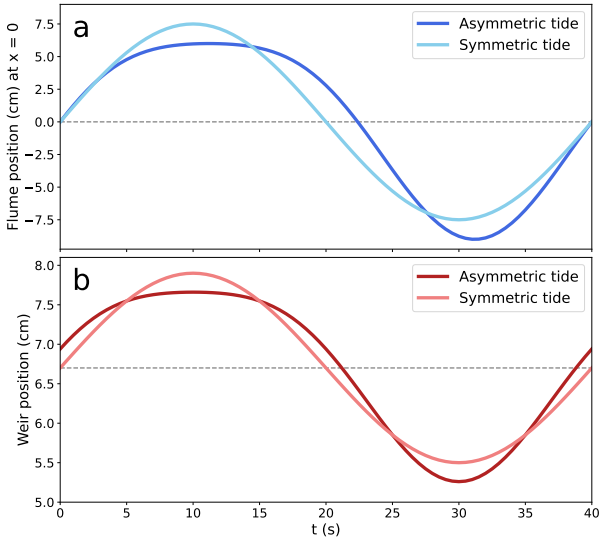

Figure 2. Metronome movement during a single emulated tidal cycle for the two different tidal settings in the dataset (Table 1). (a) The tilt of the flume at $x = 0$ m (Eq. 1). (b) The movement of the weir at $x \approx 20.35$ m (Eq. 2).

$$z_{x,t} = \left(\frac{\frac{L}{2} - (x - x_0)}{\frac{L}{2}}\right)\left(a_1 \sin\left(\frac{2\pi(t - t_s)}{T}\right) + a_2 \sin\left(\frac{2N\pi(t - t_s)}{T} + \phi\right)\right) \quad (1)$$

in which $L = 20$ m is the length of the flume along the x-axis, $x_0 = 0$ m is the x-coordinate at the origin of the coordinate reference system (upstream boundary), a_1, a_2 are amplitudes of tilt movement, t_s time shift, N frequency multiplier, and ϕ phase shift. Table 1 provides the values for these parameters for both the asymmetric and symmetric tidal settings. Note that for the symmetric tide, the second sine component of Eq. 1 becomes zero. For asymmetric tide, the time shift $t_s = 1.192$ ensures that $z_{x,t} = 0$ for $t = 0$ at all x-coordinates. Note that $z_{x,t} = 0$ for all values of t at the tilting axis ($x = 10$ m). Fig. 2.a shows $z_{x,t}$ for $x = 0$ m for both tidal settings. Accordingly, each tidal cycle starts with the ebb stage, lasting 22.5 s for asymmetric tide, and 20 s for symmetric tide.

The Metronome avoids rapid outflow during the ebb stage and excessive downstream flooding at the seaside during the flood stage that would be caused by tilting without sea-level control. To this end, the overflowing weir (situated at $x \approx 20.35$ m) moves up and down in counter-phase to the tilt movement, with position z_{wt} (in m) following Eq. 2 (also see Fig. 2.b):

$$z_{wt} = z_{w0} + a_{w1} \sin\left(\frac{2\pi t}{T}\right) + a_{w2} \sin\left(\frac{2N\pi t}{T} + \phi\right) \quad (2)$$

in which a_{w1}, a_{w2} are the amplitudes of weir movement, and z_{w0} is the initial weir level, set at 0.067 m. Note that for asymmetric tilt, ϕ causes the initial weir position to equal $z_{w,t=0} \approx 0.069$ m (Fig. 2.b). It is not critical to include a time shift t_s for

https://doi.org/10.5194/essd-2026-427
Preprint. Discussion started: 23 June 2026

Open Access Earth System Science Data Discussions

the weir movement in Eq. 2 (see Kleinhans et al., 2017b). The values of the relevant parameters for asymmetric and symmetric tilt are provided in Table 1. Furthermore, the second sine component of Eq. 2 also becomes zero for symmetric tide.

Table 1. Overview of the fixed parameters for asymmetric and symmetric tidal settings in Eqs. 1-2.

Parameter	Asymmetric tide	Symmetric tide
a_1 (m)	0.075	0.075
a_2 (m)	0.015	0
a_{w1} (m)	0.012	0.012
a_{w2} (m)	0.0024	0
t_s (s)	1.192	0
N (-)	2	1
ϕ (rad)	$\pi/2$	0
L (m)	20	20
x_0 (m)	0	0
T (s)	40	40
z_{w0} (m)	0.067	0.067

To prevent upstream flooding during the flood stage, the river pump is only activated during the ebb stage (a total of 22.5 s for asymmetric tilt and 20 s for symmetric tilt). For all experiments, the river discharge is fixed at 0.1 L/s, which is low compared to the tidal prism (Leuven et al., 2018), as is typically the case for natural tide-dominated estuaries (Dalrymple and Choi, 2007). Furthermore, a wave maker is situated at $x = 20$ m, covering the full 3 m length of the y-axis. This wave maker is a horizontal paddle which is activated during the flood stage, generating waves with an amplitude of $\sim$0.03 m and a frequency of 2 Hz. This wave maker causes wave stirring that enhances landward and alongshore sediment transport, which removes the tendency to form excessive delta lobes and delta growth, allowing for longer duration of experiments (Leuven et al., 2018). We refer to Kleinhans et al. (2017b), Leuven et al. (2018), and Braat et al. (2019) for more detailed descriptions of the Metronome facility, its functioning, scaling to natural systems, and the grain size distribution of the used sand and, for the complementary river experiments, the crushed nutshell.

3 Instrumentation

Relevant for this dataset are three different types of sensors, situated $\sim$4 m above the facility (Fig. 1.c-e). More broad descriptions of these sensors are provided in Nota et al. (2026d). Important is a rail-supported gantry system, which covers the full x-axis of the facility at $y \approx 1.5$ m (Fig. 1.d-e). Note that the large volume of raw data collected by the sensors described in this section are not included in the presented dataset (Nota et al., 2026a). The raw data for a single experiment (Exp054, Pilot 1) are included in a different publicly available dataset (Nota et al., 2025) as part of our earlier study (Nota et al., 2026d).

https://doi.org/10.5194/essd-2026-427
Preprint. Discussion started: 23 June 2026


Open Access Earth System Science Data Discussions

3.1 DSLR camera

Mounted to the gantry is a Digital Single-Lens Reflex (DSLR) camera (Canon EOS 750D; 4 Mpixel sensor; Fig. 1.d-e). We collect sequential nadir imagery with higher spatial resolution from the DSLR camera by running the gantry in stop-and-go-mode at intervals of 0.5 m. This results in imagery with a front overlap of $\sim$80%. DSLR surveys are only conducted when experiments are paused, at varying intervals of tidal cycles (commonly 1000 cycles). First, a DSLR survey is conducted over a wet bed with still water, after which the facility is carefully drained to conduct a dry bed survey. The tilting of the flume and the rapidly changing tidal flows do not allow for such surveys during a running experiment.

3.2 Line laserscanner

The gantry also contains a line laser triangulation system, consisting of an obliquely positioned 3D camera, and a 660 nm laser module with Powell lens (based on Automation Technology C5-4090-GIGE; Fig. 1.d-e). Under unlighted conditions, the gantry is continuously and slowly moving while the laser module projects a nadir laser sheet on a dry sand bed, parallel to the y-axis. The morphology-dependent reflection of the laser sheet on the bed is registered by the 3D camera, storing the raw elevation data in gridded stacked scanlines. As the experiment also needs to be paused for Laserscan survey, dry and wet bed DSLR surveys are usually conducted at the same experimental timestep as laserscans.

3.3 Overhead cameras

Fixed to the ceiling are seven industrial digital "overhead" cameras (Allied Vision Mako G419C; Fig. 1.c-e), roughly equally spaced from each other at $y \approx 1.7$ m. The overhead cameras are triggered simultaneously, by default collecting nadir imagery ($\sim$20% overlap) at fixed intervals of 20 tidal cycles when the facility is in exactly the horizontal position between the ebb and flood stage ($t = 22.5$ s for asymmetric tide, and $t = 20$ s for symmetric tide; Fig. 2.a; Eq. 1). We refer to this type of overhead imagery as *interval*. Furthermore, the overhead cameras are occasionally triggered to collect burst imagery at a set frequency. For this burst imagery, we distinguish two types. First, there are bursts of 40 images at 1 Hz (referred to as *1Hz*) triggered at $t = 1$ s, as such covering each second for a few consecutive tidal cycles (typically 7-10 in total). Second, there are bursts of 10 images at 25 Hz (referred to as *PIV*). These images are taken during a few cycles (covering each step of 5 s at least twice) after the water surface was sprinkled with floating plastic particles ($d \sim 5$ mm). The high frequency of these bursts allow for determining surface water velocities through large-scale surface Particle Image Velocimetry (PIV; Thielicke and Sonntag, 2021).

Because the overhead images are taken simultaneously, the supporting cart used for smoothening the bed is always included in the imagery (at $x = 0$ m; Fig. 1.a). Gantry surveys for DSLR imagery and laserscans are paused midway, after which the supporting cart is moved so it is not included in these surveys (Fig. 1.b&f).

https://doi.org/10.5194/essd-2026-427
Preprint. Discussion started: 23 June 2026

Open Access Earth System Science Data Discussions

4 Data processing methods

Here we briefly describe the methods we used for obtaining the processed and derived data that are available in the dataset. The developments of these methods have been the main study objectives in our previous studies, in which they are extensively covered, including quantification and evaluation of uncertainties (Nota et al., 2026b, d, and supplementary material therein). All files in the dataset have been processed within the coordinate system of the facility, from $x = 0$ m until $x = 20$ m, and $y = 0$ m until $y = 3$ m, with the origin at the upstream boundary on the left of the flume (looking downstream) (Fig. 1.a).

4.1 DSLR and overhead imagery into Orthomosaics

The DSLR and all types of overhead imagery are processed in the same way through *Base model alignment* (Nota et al., 2026d). This is a rapid and automated Structure-from-Motion (SfM) photogrammetry procedure, aligning each individual overhead series or DSLR survey to an idealized fixed 3D base model of the facility in Agisoft Metashape (v.2.0.4). This assures that all series and surveys are optimally aligned to the single reference base model geometry (Nota et al., 2026d). After alignment, orthomosaics are extracted by only enabling the imagery of the overhead series or DSLR survey (Fig 1.a-b; Fig. 3; Fig. 4.a&d). DSLR and *PIV* overhead orthomosaics are computed at a 5 mm resolution. *Interval* and *1Hz* overhead orthomosaics are computed at both 5 and 25 mm resolution.

4.2 Laserscans into DEMs and planform masks

The raw gridded laserscan data is processed into Digital Elevation Models (DEMs; Fig. 1.f) following the *Base model geometry-based laserscan* workflow described in Nota et al. (2026d). This is a triangulation method solving 3D coordinates through computer graphics algebra using spatially varying sensor positions and orientations that have been extracted from the aforementioned base model. Accordingly, the orthomosaics and DEMs are independently processed, yet constrained by the same base model geometry. For the laserscan DEMs, this assures optimal relative alignment with orthomosaics, as well as optimal vertical spatial accuracy. These accuracies are 1.9 mm for 25 mm grid size, and 2.1 mm for 5 mm grid size (confidence of 99.7%; Nota et al., 2026d). These values are sufficient considering that the morphological features are in the order of centimeters (Nota et al., 2026d).

Most of the experiments in the dataset have fixed planforms (Section 5; Supplementary material S2). Therefore, these experiments consist partially of inactive beds in which there is no morphological development (Fig. 1.a). For the purpose of deriving the water depth maps from *interval* and *1Hz* overhead orthomosaics (Section 4.3), it is convenient to mask out these regions, as well as the areas covering the supporting cart and the sea (Fig. 1.a&g Nota et al., 2026b). Such masks are computed at 25 mm resolution, typically by setting a single elevation threshold in the initial flat bed timestep of a laserscan DEM, with a single cell buffer that reduces the planform area to account for uncertainties in relative alignment and slight movement of fixed banks during an experiment. *Ad hoc* interference was required for some experiments a to properly align a mask to an experimental dataset of overhead orthomosaics. This was necessary for experiments where without fixed banks or no initial flat bed.

https://doi.org/10.5194/essd-2026-427
Preprint. Discussion started: 23 June 2026

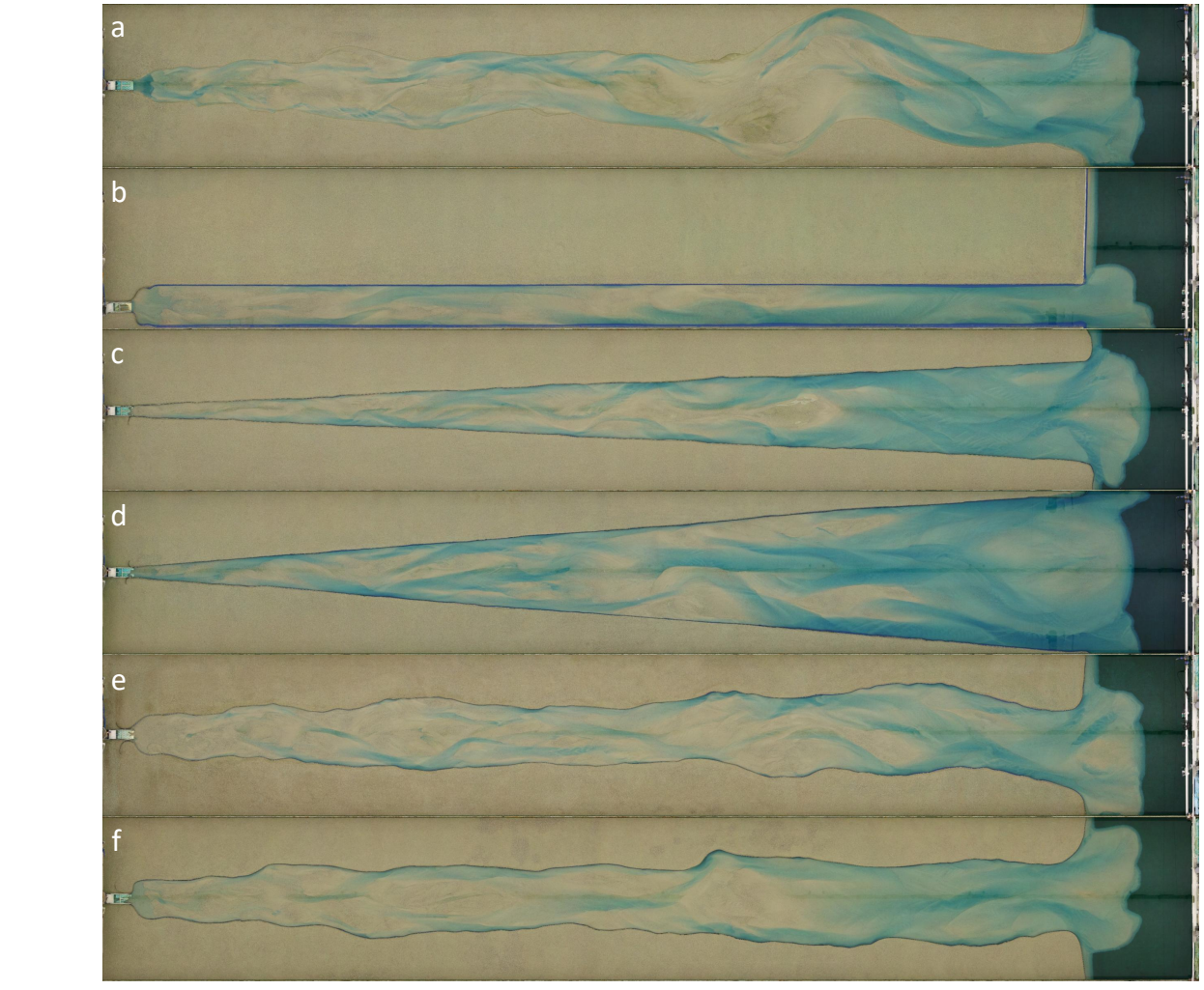

Figure 3. DSLR orthomosaics illustrating the subdivision of the experimental dataset into the various planforms. (a) Control runs without fixed banks; (b) Narrow fixed planform; (c) Seaward widening fixed planform narrow; (d) Seaward widening fixed planform wide; (e) Naturally formed fixed planform 1: perturbations on initial conditions; (f) Naturally formed fixed planform 2: tidal symmetry. The complementary river experiments are not included here.

https://doi.org/10.5194/essd-2026-427
Preprint. Discussion started: 23 June 2026


Open Access Earth System Science Data Discussions

4.3 Orthomosaics into water depth maps

From the color values of the *interval* and *1Hz* overhead orthomosaics at 25 mm resolution, we have calculated water depth maps following a workflow involving predictive models trained through machine learning (Nota et al., 2026b). For 6 different dye concentrations between 0 mg/L and 5 mg/L, two Random Forest models were trained. These dye concentrations have been established through our spectrophotometry protocol (Section 2). The workflow follows a hierarchical approach. First, a classifier model predicts which cells in the masked area are dry and wet. Second, for the wet cells specifically, a regressor model predicts the water depths (Fig. 1.g & Fig. 4.b).

For the models trained at dye concentrations between 1 mg/L and 5 mg/L, we found satisfactory and similar performances, with Peirce Skill scores of the classifier models at $\sim$0.98, and RMSE of the Regressor models at $\sim$3 mm with a negligible Bias (Nota et al., 2026b). These metrics become slightly more uncertain when validation occurs on data with experimental morphology, due to deviations with dye concentration and increased area of dry/wet interface, which is more difficult to correctly predict due to the vertical uncertainty of the input DEM (Section 4.2). In Nota et al. (2026b) we argue that this is not problematic, as the locations of deeper channels are generally morphologically more interesting to study, and deviations in dye concentration still result in linear relationships between actual and predicted water depths. We refer to Nota et al. (2026b) for a full description on how these models were trained and validated. The models, codes, training data, and validation data of this study are available in Nota et al. (2026c).

4.4 Timelapses from orthomosaics and water depth maps

For all *interval* and *1Hz* overhead orthomosaics, as well as their derived water depth maps, we have computed timelapses, indicating lab experiment number, the index of the tidal cycles, and for the *1Hz* specifically, the second within the tidal cycle. Occasionally, we have collected a set of *1Hz* overhead imagery with the *PIV* plastic particles. This frequency is too low to determine water surface velocities through PIV, so these timelapses only illustrate how PIV works.

5 Dataset

The dataset that belongs to this paper (Nota et al., 2026a) consists of the processed data described in Section 4, covering a total of 19 physical scale experiments of estuaries, including 3 pilot runs. The dataset represents almost 230,000 emulated experimental tidal cycles within the Metronome, covering $\sim$110 days of non-stop running the facility. We subdivide the dataset into six different planforms (Fig. 3), most of which are fixed by blue rough sandpaper (median grain size of 1 mm). The dataset moreover includes: (i) repeat experiments with the same initial and boundary conditions; (ii) experiments with initial bed perturbations as compared to a flat bed setup; and (iii) experiments with varying tidal settings. Each individual experiment is described in more detail in Supplementary Section S2, including the relevant peculiarities, sensor failures, oversights, or any other unexpected events to which such laboratory work is inevitably prone. Additionally, each experimental folder contains an unrefined log text file, which we maintained daily while conducting the actual experiments. Finally, the dataset includes two

https://doi.org/10.5194/essd-2026-427
Preprint. Discussion started: 23 June 2026

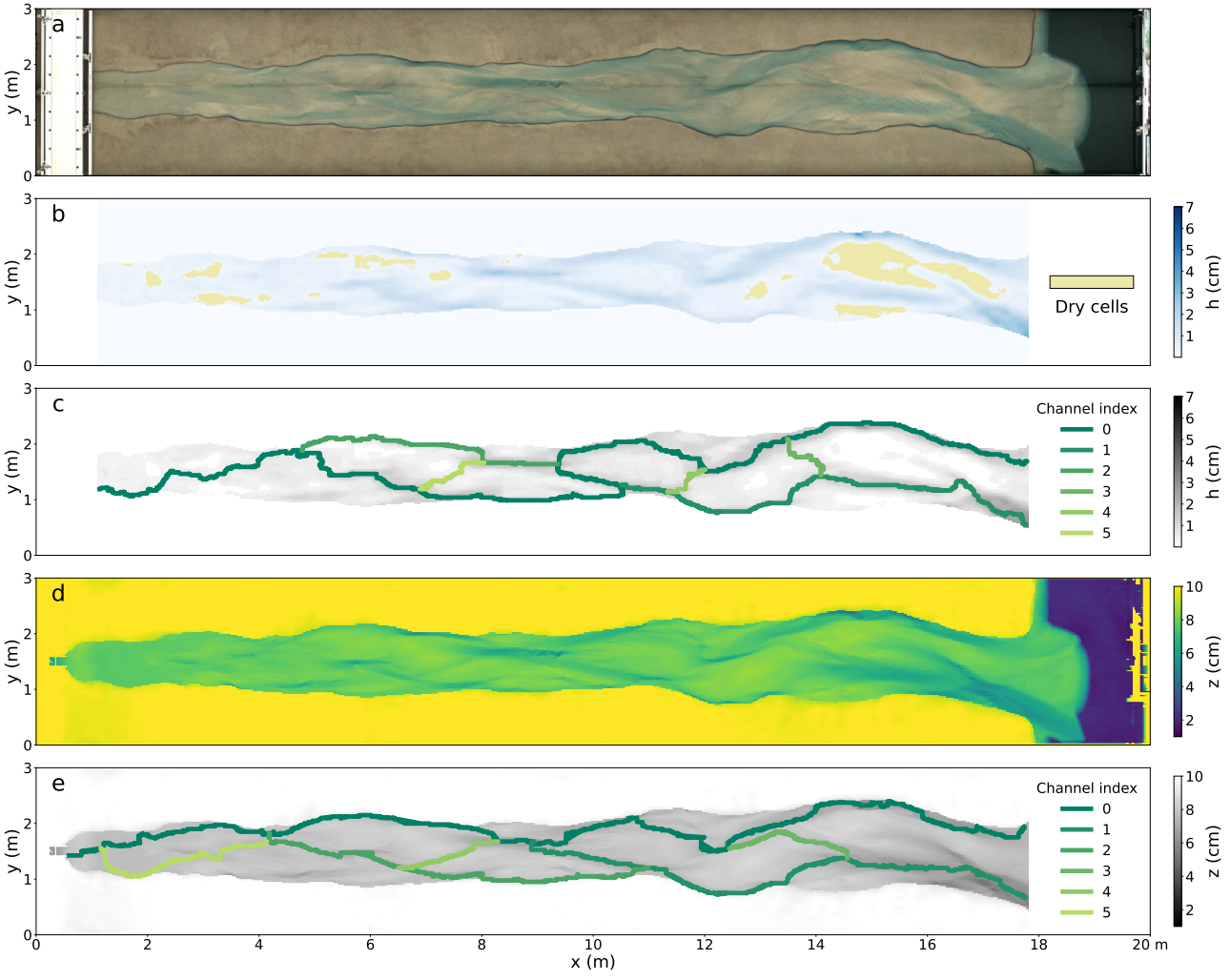

Figure 4. Illustration of applicability for extracting channel networks from TopoTide (Sonke, 2025) for a specific timestep (Exp054 Pilot1, Cycles 00999 & 01000): (a-c) Overhead water depth map at cycle 00999; and (d-e) laserscan DEM at cycle 01000. (a) *Interval* overhead orthomosaic. (b) Water depth map from ML models. (c) Channel network from water depth map in panel b. (d) DEM. (e) Channel network from DEM in panel d. Panels b-e have a resolution of 25 mm. The orthomosaic in panel a has a resolution of 5 mm for illustrative purposes.

https://doi.org/10.5194/essd-2026-427
Preprint. Discussion started: 23 June 2026

complementary river experiments at a fixed slope with a transversely moving river inlet (following Van Dijk et al., 2012; Van de Lageweg et al., 2016). The first river experiment formed a braiding river. The second river experiment showed a tendency to meander when crushed nutshell was added as suspended, floodplain-forming sediment (following Braat et al., 2019).

The data of each experiment are stored in a separate folder that includes the experimental lab number (between 052 and 081). These folders include, when relevant: (i) DEMs (Section 4.2); (ii) Planform masks (Section 4.2); (iii) DSLR and the three types of overhead orthomosaics (Section 4.1); (iv) water depth maps derived from *interval* and *1Hz* overhead orthomosaics (Section 4.3); and (v) timelapse videos from the available *interval* and *1Hz* overhead orthomosaics and water depth maps (Section 4.4). Tabular overviews on the available data for each of these experiments are provided in Supplementary Section S1. This includes the number of files per section and the relevant ranges of tidal cycles that are covered by the different types of overhead orthomosaics (Section 3.3). When considering research options, we recommend to first read the supplementary material of this paper, and observe the available timelapses for the experiments of interest.

6 Potential for analyses with the dataset

We present a large dataset of physical scale experiments of estuaries conducted in the Metronome facility, covering various planforms, perturbations and two different tidal settings. Besides, two complementary experiments of a braided and meandering river are included. The dataset contains distributed laserscan DEMs, as well as temporally dense orthomosaics and water depth maps that are optimally relatively aligned as they are processed through a single fixed base model geometry (Nota et al., 2026d). The files in the dataset capture the morphological change that happened during these experiments over various timescales. Accordingly, this experimental dataset can be useful for numerous morphological studies on the development of estuaries in response to embankments, tidal settings, perturbations and planform shape.

For instance, volume changes can be determined though analyzing timeseries of DEMs or *interval* water depth maps. The large amount of data can also be used for machine learning implementations other than determining water depths (Nota et al., 2026b), such as predicting sediment transport (Bhattacharya et al., 2007). Furthermore, the complementary river experiments in the dataset allow for a comparison of morphological development and scaling between experimental rivers and estuaries. Our recent advancements in data processing (Nota et al., 2026b, d) also provide new opportunities for quantitative research on experimental rivers (Leenman and Eaton, 2024). Moreover, with the complementary river experiments, it is possible to study the potential effects of periodic tilting of the facility for the estuarine experiments, compared to a conventional setup of fixed slope (see also Supplementary material S3).

The elevation data from DEMs or rates of change in water depths for the experiments, including various types of perturbations, can be used to investigate fluvial and estuarine bar theory on the formation and development of different types of bars and effects of topographic forcing (Tambroni et al., 2005; Leuven et al., 2018; Crosato and Mosselman, 2020; Ragno et al., 2021; Southgate, 2025). Furthermore, several experiments have a repeat experiment conducted under the same initial flat bed conditions, allowing for analysis on chaos theory and repeatability of these experimental estuaries (Adams et al., 2025). A tool that can be used for such analysis is TopoTide (Sonke et al., 2022; Sonke, 2025), which is able to extract channel networks

https://doi.org/10.5194/essd-2026-427
Preprint. Discussion started: 23 June 2026

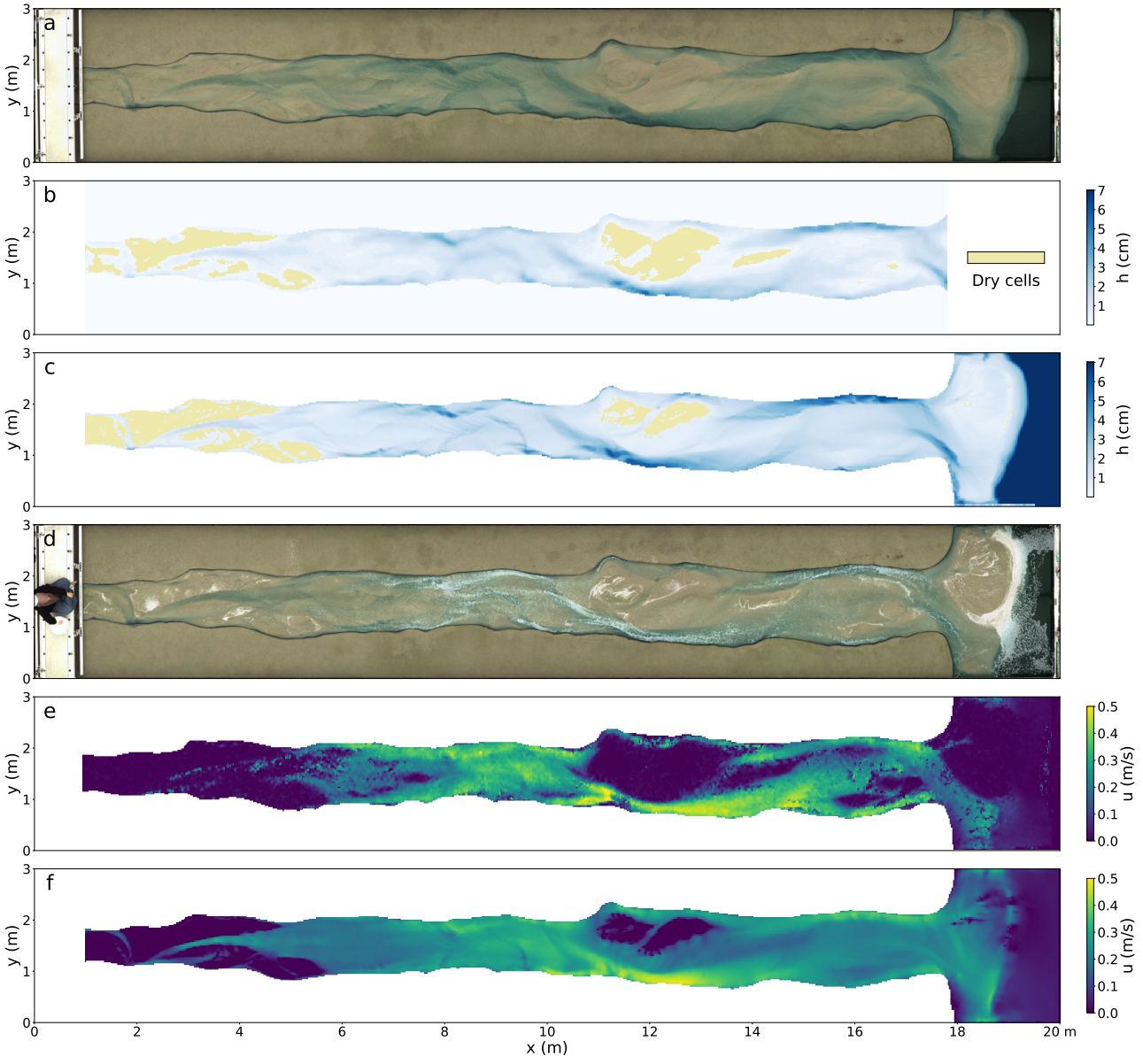

Figure 5. Illustration of applicability for the verification of the numerical model XBeach (Roelvink et al., 2010) on the dataset at a specific moment within the tidal cycle ($t = 15$ s) for a specific timestep (Exp077, Cycles 12680 & 12693) for: (a-c) 1Hz imagery at cycle 12680; and (d-f) PIV imagery at cycle 12693. (a) *1Hz* overhead orthomosaic. (b) Water depth map. (c) Modelled water depths in XBeach. (d) *PIV* overhead orthomosaic. (e) Determined surface water u-velocities from *PIV* orthomosaics (including panel d) within PIVLab software (Thielicke and Sonntag, 2021). (f) Modelled surface water u-velocities in XBeach. Panels b and e are computed through data-based analysis on orthomosaic imagery. Panels c and f are numerically modelled results using a laserscan DEM and tidal settings (Fig. 2; Supplementary material S3) as input. The orthomosaic in panel a has a resolution of 5 mm for illustrative purposes.

https://doi.org/10.5194/essd-2026-427
Preprint. Discussion started: 23 June 2026

for both water depth maps and DEMs (Fig. 4). For the *interval* water depth maps specifically, this allows for quantification of migrating channel networks for small to large timescales (Nota et al., 2026b).

Finally, the dataset consists of several configurations that can be combined to verify and calibrate coastal numerical models (Weisscher et al., 2020). Fig. 5 provides an illustration of our efforts to represent the Metronome facility within the model suite XBeach (Roelvink et al., 2009, 2010). Such verification can occur through comparing water depth maps derived from *1Hz* overhead orthomosaics with modelled water depths (Fig. 5.a-c). Modelled flow velocities can be compared to surface water velocities that have been determined from *PIV* overhead orhomosaics (Fig. 5.d-f) through PIV software (e.g. PIVLab; Thielicke and Sonntag, 2021), assuming the law of the wall and a calibrated roughness length. For successful implementation of such a numerical model on this facility, the water levels and tilt movement that induce the tidal flows have to be implemented (Fig. 2; Eqs. 1-2; Supplementary material S3). To conclude, the large amount of elevation and depth data in this dataset allows for opportunities to implement this dataset in various disciplines, including fluvial geomorphology, numerical modelling, spatial statistics, and machine learning.

Code and data availability

The dataset presented in this study is available at the online repository of Utrecht University (https://public.yoda.uu.nl/geo/UU01/KKEUY5.html; Nota et al., 2026a). Included are python scripts that can be used to load all experimental data and their relevant metadata. For an experimental dataset with raw data, and code to process it, we refer to Nota et al. (2025) (https://public.yoda.uu.nl/geo/UU01/SGM22N.html). The random forest models that were used to compute water depth maps form overhead orthomosaics are available at Nota et al. (2026c) (https://public.yoda.uu.nl/geo/UU01/2XBVKK.html). This dataset also includes the training and validation data of these models. Furthermore, all our codes are uploaded and updated on our GitHub page (https://github.com/UtrechtRiversEstuaries). Additionally, we have implemented varying water levels and tilt functions in a separate version of the model XBeach, which is available at: https://github.com/saeb-faraji-gargari/Xbeach_dev_Moving_boundary/tree/20240110_XBeach_v4_20251114.

Author contributions

EN, MK, YL, LBe, and SB contributed to the design of the experiments. EN, YL, LBe, MU, MW, ZN, SB, EA, LG, JM, BA, JD, and JR conducted the experiments and collected the raw data. MM, HM, AE, BD, LBr, and SF provided technical support. EN, BA, MN, SF, MU, YL, MW, SB, DL, JR, MM, and MK have have been involved in the development of the various methods and software for data processing that resulted in the database. MK, VB, MM, HM, AE, and BD provided the relevant resources. EN, VB, and MK were responsible for the data curation. MK, EN, SF, and MN provided supervision in the multiple projects combined in this dataset. YL, LBe, MU, MW, ZN, SB and DL have contributed as part of their MSc thesis projects. EA, LG, and JM have contributed as part of their BSc thesis projects. EN processed all data, made the visualizations and wrote the original draft. EN, MK, SF, VB, MN, LBe, MW, YL, SB, BA, JD, and JR reviewed and edited the manuscript.

https://doi.org/10.5194/essd-2026-427
Preprint. Discussion started: 23 June 2026

Open Access Earth System Science Data Discussions

Competing interests

The authors declare that they have no competing interests.

Acknowledgements

This research is supported by the Dutch Research Council (NWO), grant OCENW.M20.089 to Bettina Speckmann (TU Eindhoven) and Maarten Kleinhans. We are grateful to Willem Sonke, Bettina Speckmann, Thijs Beurskens, Tim Ophelders, Kevin Verbeek, and Anna Schenfisch (Applied Geometric Algorithms group, TU Eindhoven) for their contributions in implementing our laboratory data in TopoTide. Furthermore, we are grateful to Dano Roelvink for the first implementation of the Metronome in XBeach, and Dano Roelvink and Maarten van der Vegt for helping out to further implement the Metronome setup in XBeach. Both projects are ongoing.

https://doi.org/10.5194/essd-2026-427
Preprint. Discussion started: 23 June 2026

References

Adams, D. L., Hassan, M. A., and Davidson, S.: The unrepeatable river: Exploring chaotic variability in laboratory channels, Earth Surf. Processes and Landforms, 50, e70 027, https://doi.org/10.1002/esp.70027, 2025.

Baar, A., Boechat Albernaz, M., Van Dijk, W., and Kleinhans, M.: Critical dependence of morphodynamic models of fluvial and tidal systems on empirical downslope sediment transport, Nat. Commun., 10, 4903, https://doi.org/10.1038/s41467-019-12753-x, 2019.

Bhattacharya, B., Price, R., and Solomatine, D.: Machine learning approach to modeling sediment transport, J. Hydraul. Eng., 133, 440–450, https://doi.org/10.1061/(ASCE)0733-9429(2007)133:4(440), 2007.

Braat, L., Leuven, J. R., Lokhorst, I. R., and Kleinhans, M. G.: Effects of estuarine mudflat formation on tidal prism and large-scale morphology in experiments, Earth Surf. Processes and Landforms, 44, 417–432, https://doi.org/10.1002/esp.4504, 2019.

Bradley, C., Bowes, M. J., Brils, J., Friedrich, J., Gault, J., Groom, S., Hein, T., Heininger, P., Michalopoulos, P., Panin, N., Schultz, M., Stanica, A., Andrei, I., Tyler, A., and Umgiesser, G.: Advancing integrated research on European river–sea systems: the DANUBIUS-RI project, Int. J. Water Resour. Dev., 34, 888–899, https://doi.org/10.1080/07900627.2017.1399107, 2018.

Cea, L. and French, J.: Bathymetric error estimation for the calibration and validation of estuarine hydrodynamic models, Estuarine Coastal Shelf Sci., 100, 124–132, https://doi.org/10.1016/j.ecss.2012.01.004, 2012.

Clark, D., Goodwin, E., Sinner, J., Ellis, J., and Singh, G.: Validation and limitations of a cumulative impact model for an estuary, Ocean Coastal Manage., 120, 88–98, https://doi.org/10.1016/j.ocecoaman.2015.11.013, 2016.

Cox, J., Lingbeek, J., Weisscher, S., and Kleinhans, M.: Effects of sea-level rise on dredging and dredged estuary morphology, J. Geophys. Res.: Earth Surf., 127, e2022JF006 790, https://doi.org/10.1029/2022JF006790, 2022.

Crosato, A. and Mosselman, E.: An integrated review of river bars for engineering, management and transdisciplinary research, Water, 12, 596, https://doi.org/10.3390/w12020596, 2020.

Dalrymple, R. W. and Choi, K.: Morphologic and facies trends through the fluvial–marine transition in tide-dominated depositional systems: a schematic framework for environmental and sequence-stratigraphic interpretation, Earth Sci. Rev, 81, 135–174, https://doi.org/10.1016/j.earscirev.2006.10.002, 2007.

Dorst, L. L., Roos, P. C., and Hulscher, S. J.: Improving a bathymetric resurvey policy with observed sea floor dynamics, J. Appl. Geod., 7, https://doi.org/10.1515/jag-2012-0035, 2013.

Dutta, S., Middelkoop, H., and Ruessink, G.: Delta-ENIGMA: an integrated large-scale research infrastructure for delta dynamics, Tech. rep., Copernicus Meetings, https://doi.org/10.5194/egusphere-egu26-13825, 2026.

Elias, E. P., Van der Spek, A. J., Wang, Z. B., Cleveringa, J., Jeuken, C. J., Taal, M., and Van der Werf, J. J.: Large-scale morphological changes and sediment budget of the Western Scheldt estuary 1955–2020: the impact of large-scale sediment management, Neth. J. Geosci., 102, e12, https://doi.org/10.1017/njg.2023.11, 2023.

Kennish, M. J.: Environmental threats and environmental future of estuaries, Environ. Conserv., 29, 78–107, https://doi.org/10.1017/S0376892902000061, 2002.

Kleinhans, M. G.: Flow discharge and sediment transport models for estimating a minimum timescale of hydrological activity and channel and delta formation on Mars, J. Geophys. Res.: Planets, 110, https://doi.org/10.1029/2005JE002521, 2005.

Kleinhans, M. G., van Dijk, W. M., van de Lageweg, W. I., Hoyal, D. C., Markies, H., van Maarseveen, M., Roosendaal, C., van Weesep, W., van Breemen, D., Hoendervoogt, R., and Cheshier, N.: Quantifiable effectiveness of experimental scaling of river-and delta morphodynamics and stratigraphy, Earth Sci. Rev, 133, 43–61, https://doi.org/10.1016/j.earscirev.2014.03.001, 2014.

https://doi.org/10.5194/essd-2026-427
Preprint. Discussion started: 23 June 2026

Kleinhans, M. G., Van Scheltinga, R. T., Van Der Vegt, M., and Markies, H.: Turning the tide: Growth and dynamics of a tidal basin and inlet in experiments, J. Geophys. Res.: Earth Surf., 120, 95–119, https://doi.org/10.1002/2014JF003127, 2015.

Kleinhans, M. G., Leuven, J. R., Braat, L., and Baar, A.: Scour holes and ripples occur below the hydraulic smooth to rough transition of movable beds, Sedimentology, 64, 1381–1401, https://doi.org/10.1111/sed.12358, 2017a.

Kleinhans, M. G., Van Der Vegt, M., Leuven, J., Braat, L., Markies, H., Simmelink, A., Roosendaal, C., Van Eijk, A., Vrijbergen, P., and Van Maarseveen, M.: Turning the tide: Comparison of tidal flow by periodic sea level fluctuation and by periodic bed tilting in scaled landscape experiments of estuaries, Earth Surf. Dyn., 5, 731–756, https://doi.org/10.5194/esurf-5-731-2017, 2017b.

Leenman, A. S. and Eaton, B. C.: Remote sensing of laboratory rivers, Earth Surf. Processes and Landforms, 49, 58–81, https://doi.org/10.1002/esp.5577, 2024.

Leuven, J. R., Braat, L., van Dijk, W. M., de Haas, T., Van Onselen, E., Ruessink, B., and Kleinhans, M. G.: Growing forced bars determine nonideal estuary planform, J. Geophys. Res.: Earth Surf., 123, 2971–2992, https://doi.org/10.1029/2018JF004718, 2018.

Leuven, J. R., Pierik, H. J., Vegt, M. v. d., Bouma, T. J., and Kleinhans, M. G.: Sea-level-rise-induced threats depend on the size of tide-influenced estuaries worldwide, Nat. Clim. Change, 9, 986–992, https://doi.org/10.1038/s41558-019-0608-4, 2019.

Lin, H., Palacios, J., Fagherazzi, S., and Fichot, C. G.: Estimating net sediment fluxes in tidal systems using sporadic data sets: Implications for using remote sensing to assess saltmarsh resilience, Geophys. Res. Lett., 53, e2025GL117 671, https://doi.org/10.1029/2025GL117671, 2026.

Montani, S., Magni, P., Shimamoto, M., Abe, N., and Okutani, K.: The effect of a tidal cycle on the dynamics of nutrients in a tidal estuary in the Seto Inland Sea, Japan, J. Oceanogr., 54, 65–76, https://doi.org/10.1007/BF02744382, 1998.

Nota, E. W., van Amstel, B. A., Nijland, W., van Maarseveen, M. C., and Kleinhans, M. G.: Data supplement to "Remote sensing of a gantry-equipped facility: optimizing accuracy by integrating SfM photogrammetry and laserscan computer graphics through fixed base model geometry" [Dataset], Yoda - Utrecht Univ., https://doi.org/10.24416/UU01-SGM22N, 2025.

Nota, E. W., Li, Y., Beyaard, L., Upson, M., Wagenaar, M. L., Nassralla, Z., Baltussen, S. J., van Amelsfort, E., Gubbels, L. M., Leahy, D., Muller, J. J., van Amstel, B. A., Donders, J. J., Rossius, J.-E., van Maarseveen, M. C., Markies, H., van Eijk, A. M., van Dam, B. D., Nussbaum, M., Faraji Gargari, S., Brunst, V., Braat, L., and Kleinhans, M. G.: Data supplement to "Experimental dataset on estuarine hydrodynamics and morphodynamics for various planforms and timescales" [Dataset], Yoda - Utrecht Univ., https://doi.org/10.24416/UU01-KKEUY5, 2026a.

Nota, E. W., Nussbaum, M., Upson, M., Leahy, D., Langenbach, J.-W. H., and Kleinhans, M. G.: Quantitative water depth determination in large experimental timeseries through combining spectrophotometry and machine learning, ESS Open Arch., https://doi.org/10.22541/essoar.177082648.88604562/v1, 2026b.

Nota, E. W., Nussbaum, M., Upson, M., Leahy, D., Langenbach, J.-W. H., and Kleinhans, M. G.: Data supplement to "Quantitative water depth determination in large experimental timeseries through combining spectrophotometry and machine learning" [Dataset], Yoda - Utrecht Univ., https://doi.org/10.24416/UU01-2XBVKK, 2026c.

Nota, E. W., van Amstel, B. A., Nijland, W., van Maarseveen, M. C., and Kleinhans, M. G.: Remote sensing of a gantry-equipped facility: optimizing accuracy by integrating SfM photogrammetry and laserscan computer graphics through fixed base model geometry, Int. J. Appl. Earth Obs. Geoinf., 146, 15 098, https://doi.org/10.1016/j.jag.2026.105098, 2026d.

Nowacki, D. J., Ogston, A. S., Nittrouer, C. A., Fricke, A. T., and Van, P. D. T.: Sediment dynamics in the lower Mekong River: Transition from tidal river to estuary, J. Geophys. Res.: Oceans, 120, 6363–6383, https://doi.org/10.1002/2015JC010754, 2015.

https://doi.org/10.5194/essd-2026-427
Preprint. Discussion started: 23 June 2026

Paola, C., Straub, K., Mohrig, D., and Reinhardt, L.: The "unreasonable effectiveness" of stratigraphic and geomorphic experiments, Earth Sci. Rev, 97, 1–43, https://doi.org/10.1016/j.earscirev.2009.05.003, 2009.

Ragno, N., Tambroni, N., and Bolla Pittaluga, M.: When and where do free bars in estuaries and tidal channels form?, J. Geophys. Res.: Earth Surf., 126, e2021JF006 196, https://doi.org/10.1029/2021JF006196, 2021.

Reynolds, O.: On Certain Laws Relating to the Regime of Rivers and Estuaries, and on the Possibility of Experiments on a Small Scale, British Association Report, 1888.

Reynolds, O., Brightmore, A. W., and Moorby, W. H.: Papers on mechanical and physical subjects, Cambridge University Press, 1901.

Roelvink, D., Reniers, A., Van Dongeren, A., De Vries, J. V. T., McCall, R., and Lescinski, J.: Modelling storm impacts on beaches, dunes and barrier islands, Coastal Eng., 56, 1133–1152, https://doi.org/10.1016/j.coastaleng.2009.08.006, 2009.

Roelvink, D., Reniers, A., Van Dongeren, A., Van Thiel de Vries, J., Lescinski, J., and McCall, R.: XBeach model description and manual, 2010.

Sonke, W.: tue-alga/topotide: 2.1.2, https://doi.org/10.5281/zenodo.15397705, 2025.

Sonke, W., Kleinhans, M. G., Speckmann, B., van Dijk, W. M., and Hiatt, M.: Alluvial connectivity in multi-channel networks in rivers and estuaries, Earth Surf. Processes and Landforms, 47, 477–490, https://doi.org/10.1002/esp.5261, 2022.

Southgate, H. N.: Free evolution in the Ginzburg-Landau equation and other complex diffusion equations, Phys. Scr., 100, 015 261, https://doi.org/10.1088/1402-4896/ad8aa0, 2025.

Tambroni, N., Bolla Pittaluga, M., and Seminara, G.: Laboratory observations of the morphodynamic evolution of tidal channels and tidal inlets, J. Geophys. Res.: Earth Surf., 110, https://doi.org/10.1029/2004JF000243, 2005.

Thielicke, W. and Sonntag, R.: Particle Image Velocimetry for MATLAB: Accuracy and enhanced algorithms in PIVlab, J. Open Res. Software, 9, https://doi.org/10.5334/jors.334, 2021.

Van de Lageweg, W. I., van Dijk, W. M., Box, D., and Kleinhans, M. G.: Archimetrics: a quantitative tool to predict three-dimensional meander belt sandbody heterogeneity, Depositional Rec., 2, 22–46, https://doi.org/10.1002/dep2.12, 2016.

Van der Wal, D. and Pye, K.: The use of historical bathymetric charts in a GIS to assess morphological change in estuaries, Geogr. J., 169, 21–31, https://doi.org/10.1111/1475-4959.04943, 2003.

Van Dijk, W. M., Van de Lageweg, W., and Kleinhans, M. G.: Experimental meandering river with chute cutoffs, J. Geophys. Res.: Earth Surf., 117, https://doi.org/10.1029/2011JF002314, 2012.

Van Maren, D., Colina Alonso, A., Engels, A., Vandenbruwaene, W., De Vet, P., Vroom, J., and Wang, Z.: Adaptation timescales of estuarine systems to human interventions, Front. Earth Sci., 11, 1111 530, https://doi.org/10.3389/feart.2023.1111530, 2023.

Weisscher, S. A., Boechat-Albernaz, M., Leuven, J. R., Van Dijk, W. M., Shimizu, Y., and Kleinhans, M. G.: Complementing scale experiments of rivers and estuaries with numerically modelled hydrodynamics, Earth Surf. Dyn., 8, 955–972, https://doi.org/10.5194/esurf-8-955-2020, 2020.

Williams, J. J. and Esteves, L. S.: Guidance on setup, calibration, and validation of hydrodynamic, wave, and sediment models for shelf seas and estuaries, Adv. Civ. Eng., 2017, 5251 902, https://doi.org/10.1155/2017/5251902, 2017.